Convergence Analysis of the Distributed Analytical Representation and Iterative Technique (DARIT-Field) for the Field Coupling to Multiconductor Transmission Lines

Convergence Analysis of the Distributed Analytical Representation and Iterative Technique (DARIT-Field) for the Field Coupling to Multiconductor Transmission Lines

Jun Guo, Yan-Zhao Xie, Ke-Jie Li, and Flavio Canavero

***Abstract*—This paper investigates the convergence and error evaluation of the distributed analytical representation and iterative technique (DARIT-field) which is a new approach for the analysis of field coupling to multiconductor transmission lines. The DARIT-field method has the advantage of high computational efficiency over the other methods. In order to know the convergence speed and the error at each iteration step of DARIT-field, an analytic expression of iterative error is derived by combining the two telegrapher's equations into a matrix equation and using the euclidean norm to explore its upper bound. The expression shows that the convergence speed is mainly influenced by three parameters, namely coupling factor (CF), terminal loads, and the line length to excitation field wavelength ratio (d/λ). The convergence speed is a function of CF, terminal loads, and the line length to excitation field wavelength ratio (d/λ). These results allow the users to make a compromise between computational cost and accuracy by selecting the number of iterations.**

***Index Terms*—Analytical solution, convergence, matrix norm, transmission line modeling, waveform relaxation.**

I. Introduction

THE electromagnetic pulse (EMP) may couple to the multiconductor transmission lines (MTLs) and induce high voltages and currents which would make serious damage to the equipments connected to MTLs. So, it is important to investigate in this kind of field-wire coupling and to predict the effects in modern electronic circuits [1]–[10]. Generally, one uses transmission line approximation method to calculate the responses of MTLs when excited by incoming EMP plane wave. However, the process contains many steps of decoupling algorithm (by means of similarity transformation) and matrix inversion which are all time-consuming tasks. The processing time will be too long for the simulation of a large number of coupled transmission lines [1]–[10].

J. Guo, Y.-Z. Xie, and K.-J. Li are with the State Key Laboratory of Electrical Insulation and Power Equipment, School of Electrical Engineering, Xi'an Jiaotong University, Xi'an 710049, China (e-mail: gjgjgj@stu.xjtu.edu.cn; yzxie@mail.xjtu.edu.cn; bensonwind@gmail.com).

F. Canavero is with the Electromagnetic Compatibility Group, Department of Electronics, Politecnico Di Torino, Turin 10129, Italy (e-mail: flavio.canavero@polito.it).

Therefore, it is important to find other ways which can avoid the need to inverse the matrix when solving transmission line equations. In 2010, Xie *et al.* proposed an approach using the distributed analytical representation and iterative technique (DARIT) method which is based on the waveform relaxation and transverse partitioning (WR-TP) for the crosstalk computation between MTLs [11]. Henceforth, this approach is named as the DARIT-crosstalk method. In 2013, Xie *et al.* extended the DARIT-crosstalk method to the DARIT-field (for the prediction of field coupling to lines) method [12]. The DARIT-field method could be employed to the area of EMP radiated field interaction with transmission lines which can avoid the need for inversing the matrix when solving MTL equations. The voltages and currents at the terminals are solved by the Baum–Liu–Tesche (BLT) equation [11], [13] at each iteration (more details of the DARIT-field see [12]). However, the method has certain limitations due to the need for more iterations to get the required accuracy in some situations, therefore, it is important to find the key factors which have profound influence on the convergence and to study the dependence of these factors on the convergence of this method.

Such concern for DARIT-field is similar to any WR process. Some convergence analyses of WR have been done in [15]–[35]. Especially in [15], it provided a rigorous conceptual and theoretical framework for explaining the convergence of WR method. In this paper, the iteration results of DARIT-field method are shown and the convergence is analyzed. An expression of relative error after nth iteration is deduced by combining the two equations of telegrapher's equations into a matrix equation and exploring the upper bound of relative error by using the matrix norm. Three key factors are found from the expression and the dependence of them is investigated. The results from the actual examples show the accuracy of the conclusion.

The rest of this paper is organized as follows. Section II describes the basic idea of the proposed DARIT-field approach and the four steps of iteration. Section III presents the derivation process of relative error formula and studies the relationship between the three key factors and the convergence. Sections IV and V present the validation examples and conclusions, respectively.

II. Outline of the DARIT-Field

The problem to be investigated is shown in Fig. 1. It consists of MTLs of length d and the number of conductors N (the

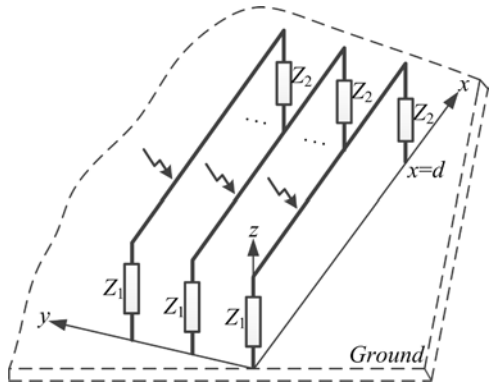

Fig. 1. Configuration of MTLs to be investigated.

reference conductor is not included), with linear loads at each end of the lines. All the lines are excited by the incoming EMP plane wave. For this problem, the load responses of voltages and currents at each line end are to be determined.

A. Basis of the Proposed Algorithm

The EMP wave is first converted to the frequency domain by fast Fourier transform (FFT). Then, the formulas are derived in frequency domain. Last, the results in the frequency domain were converted back to the time domain by IFFT.

The Telegrapher's equations of the MTLs in the frequency domain are described by a set of differential equations in the following form:

$$\begin{aligned}\frac{d\mathbf{V}(x,\omega)}{dx}+\mathbf{Z}'(\omega)\mathbf{I}(x,\omega)&=\mathbf{V}'(x,\omega)\\ \frac{d\mathbf{I}(x,\omega)}{dx}+\mathbf{Y}'(\omega)\mathbf{V}(x,\omega)&=\mathbf{I}'(x,\omega)\end{aligned}\tag{1}$$

where $\mathbf{V}(x,\omega)$ and $\mathbf{I}(x,\omega)$ are the vectors of the N voltages and currents on the lines. $\mathbf{V}'(x,\omega)$ and $\mathbf{I}'(x,\omega)$ are the source terms whose detailed expressions depend upon the coupling model used, e.g., Taylor model (used in this paper), Agrawal Model, and Rachidi Model. $\mathbf{Z}'$ and $\mathbf{Y}'$ are the $N\times N$ matrices of the line impedances and admittances which, in general, are frequency-dependent and can be written as

$$\mathbf{Z}'(\omega)=\mathbf{R}'(\omega)+j\omega\mathbf{L}'(\omega),\mathbf{Y}'(\omega)=\mathbf{G}'(\omega)+j\omega\mathbf{C}'(\omega).\tag{2}$$

The Telegrapher's equations in (1) for line i could be expressed as follows:

$$\begin{aligned}\frac{dv_i(x,\omega)}{dx}+z'_{ii}(\omega)i_i(x,\omega)&=-\sum_{\substack{j=1\\j\neq i}}^{N}z'_{ij}(\omega)i_j(x,\omega)+V'_i(x,\omega)\\ \frac{di_i(x,\omega)}{dx}+y'_{ii}(\omega)v_i(x,\omega)&=-\sum_{\substack{j=1\\j\neq i}}^{N}y'_{ij}(\omega)v_j(x,\omega)+I'_i(x,\omega)\end{aligned}\tag{3}$$

where $V'_i(x,\omega)$ and $I'_i(x,\omega)$ are the general source terms of line i due to the incoming EMP wave. The summation terms in (3) are the neighboring effects on line i due to the coupling of other adjacent lines. By applying waveform relaxation techniques to (3), we obtain a recursive set of decoupled differential equations in the frequency domain

$$\begin{aligned}\frac{dv_i^{(r+1)}(x,\omega)}{dx}+z'_{ii}(\omega)i_i^{(r+1)}(x,\omega)&=-\sum_{\substack{j=1\\j\neq i}}^{N}z'_{ij}(\omega)i_j^{(r)}\\&\quad(x,\omega)+V'_i(x,\omega)\\ \frac{di_i^{(r+1)}(x,\omega)}{dx}+y'_{ii}(\omega)v_i^{(r+1)}(x,\omega)&=-\sum_{\substack{j=1\\j\neq i}}^{N}y'_{ij}(\omega)v_j^{(r)}\\&\quad(x,\omega)+I'_i(x,\omega)\end{aligned}\tag{4}$$

where r represents the rth iteration, $r\geq 0$.

Hereafter, we simply present the derived formulas of two iterations. In order to make a distinction between different iterations, the general subscript index at these two iterations are represented by m, n, respectively.

B. Iteration 1

The general subscript index of this step is m. At this iteration, there are no coupling effects due to the neighboring line since the initial states of the lines are zeros. The only exciting source is from the illuminating EMP wave. Therefore, (4) could be simplified and rewritten as

$$\begin{aligned}\frac{dv_m^{(1)}(x,\omega)}{dx}+z'_{mm}(\omega)i_m^{(1)}(x,\omega)&=V'_m(x,\omega)\\ \frac{di_m^{(1)}(x,\omega)}{dx}+y'_{mm}(\omega)v_m^{(1)}(x,\omega)&=I'_m(x,\omega).\end{aligned}\tag{5}$$

C. Iteration 2

The general subscript index of this step is n. At this iteration, each line is excited by the incoming EMP wave and the coupling effects of all the other adjacent lines. For the voltages and currents on the nth line, we have

$$\begin{aligned}\frac{dv_n^{(2)}(x)}{dx}+z'_{nn}i_n^{(2)}(x)&=-\sum_{\substack{m=1\\m\neq n}}^{N}z'_{nm}i_m^{(1)}(x)+V'_n(x)\\ \frac{di_n^{(2)}(x)}{dx}+y'_{nn}v_n^{(2)}(x)&=-\sum_{\substack{m=1\\m\neq n}}^{N}y'_{nm}v_m^{(1)}(x)+I'_n(x).\end{aligned}\tag{6}$$

D. More Iterations

The calculation method of more iterations is the same as in Iteration 2. The Telegrapher's equations for these two steps are the same as in Iteration 2 except the indexes.

III. Convergence of the DARIT-Field

A. Solution of Equation

The convergence analysis starts from the telegrapher's (1). In order to solve the differential equations, let us take the concept of the combined voltage wave to represent the distribution of voltage and current on the lines. Denoting that

$$\begin{aligned}\mathbf{W}_+(x,\omega) &= \mathbf{V}(x,\omega) + \mathbf{Z_c}(\omega)\mathbf{I}(x,\omega)\\ \mathbf{W}_-(x,\omega) &= \mathbf{V}(x,\omega) - \mathbf{Z_c}(\omega)\mathbf{I}(x,\omega)\end{aligned} \tag{7}$$

where

$$\mathbf{Z_c}(\omega) = \sqrt{\mathbf{Z}'(\omega)\mathbf{Y}'(\omega)^{-1}} \tag{8}$$

is the characteristic impedance of MTLs.

Taking (7) to (1) and simplifying the expression, it can be written as

$$\begin{aligned}\frac{d\mathbf{W}_+(x,\omega)}{dx} + \boldsymbol{\gamma}(\omega)\mathbf{W}_+(x,\omega) &= \mathbf{W}'_+(x,\omega)\\ \frac{d\mathbf{W}_-(x,\omega)}{dx} - \boldsymbol{\gamma}(\omega)\mathbf{W}_-(x,\omega) &= \mathbf{W}'_-(x,\omega)\end{aligned} \tag{9}$$

where

$$\begin{aligned}\mathbf{W}'_+(x,\omega) &= \mathbf{V}'(x,\omega) + \mathbf{Z_c}(\omega)\mathbf{I}'(x,\omega)\\ \mathbf{W}'_-(x,\omega) &= \mathbf{V}'(x,\omega) - \mathbf{Z_c}(\omega)\mathbf{I}'(x,\omega)\\ \boldsymbol{\gamma}(\omega) &= \sqrt{\mathbf{Z}'(\omega)\mathbf{Y}'(\omega)}.\end{aligned} \tag{10}$$

Looking at the parameter $\boldsymbol{\gamma}(\omega)$, it is the propagation constant of MTLs and is split into a diagonal part and a nondiagonal part. The diagonal part will be denoted with $\boldsymbol{\gamma_D}(\omega)$ and the nondiagonal part will be denoted with $\boldsymbol{\gamma_N}(\omega)$. Taking them into (9), it can be written as

$$\begin{aligned}\frac{d\mathbf{W}_+(x,\omega)}{dx} + \boldsymbol{\gamma_D}(\omega)\mathbf{W}_+(x,\omega) &= \mathbf{W}'_+(x,\omega)\\ &\quad - \boldsymbol{\gamma_N}(\omega)\mathbf{W}_+(x,\omega)\\ \frac{d\mathbf{W}_-(x,\omega)}{dx} - \boldsymbol{\gamma_D}(\omega)\mathbf{W}_-(x,\omega) &= \mathbf{W}'_-(x,\omega)\\ &\quad + \boldsymbol{\gamma_N}(\omega)\mathbf{W}_-(x,\omega).\end{aligned} \tag{11}$$

The two first-order equations mentioned previously can be combined in a single first-order equation, in which the $\boldsymbol{\Psi}(x,\omega)$ and the $\boldsymbol{\Psi}'(x,\omega)$ are vectors with $2N$ elements

$$\frac{d\boldsymbol{\Psi}(x,\omega)}{dx} + \mathbf{D}(\omega)\boldsymbol{\Psi}(x,\omega) = \boldsymbol{\Psi}'(x,\omega) - \mathbf{N}(\omega)\boldsymbol{\Psi}(x,\omega) \tag{12}$$

where we have defined

$$\begin{aligned}\boldsymbol{\Psi}(x,\omega) &= \begin{bmatrix}\mathbf{W}_+(x,\omega)\\ \mathbf{W}_-(x,\omega)\end{bmatrix} \in \mathbf{R}^{2N}\\ \boldsymbol{\Psi}'(x,\omega) &= \begin{bmatrix}\mathbf{W}'_+(x,\omega)\\ \mathbf{W}'_-(x,\omega)\end{bmatrix} \in \mathbf{R}^{2N}\end{aligned} \tag{13}$$

and

$$\begin{aligned}\mathbf{D}(\omega) &= \begin{bmatrix}\boldsymbol{\gamma_D}(\omega) & \mathbf{0}\\ \mathbf{0} & -\boldsymbol{\gamma_D}(\omega)\end{bmatrix} \in \mathbf{R}^{2N} \times \mathbf{R}^{2N}\\ \mathbf{N}(\omega) &= \begin{bmatrix}\boldsymbol{\gamma_N}(\omega) & \mathbf{0}\\ \mathbf{0} & -\boldsymbol{\gamma_N}(\omega)\end{bmatrix} \in \mathbf{R}^{2N} \times \mathbf{R}^{2N}.\end{aligned} \tag{14}$$

If the term $-\mathbf{N}(\omega)\boldsymbol{\Psi}(x,\omega)$ in (12) is considered as an input excitation now, the general solution of (12) can be solved as

$$\begin{aligned}\boldsymbol{\Psi}(x,\omega) = e^{-\mathbf{D}(\omega)x}\boldsymbol{\Psi}(x_0,\omega) + \int_{x_0}^{x} e^{-\mathbf{D}(\omega)(x-x')}\big[\boldsymbol{\Psi}'(x',\omega)\\ - \mathbf{N}(\omega)\boldsymbol{\Psi}(x',\omega)\big]dx'.\end{aligned} \tag{15}$$

The parameter $\boldsymbol{\Psi}(x_0,\omega)$ is the initial vector of $\boldsymbol{\Psi}(x,\omega)$ that corresponds to $\mathbf{W}_+(0,\omega)$ on near-end and $\mathbf{W}_-(d,\omega)$ on far-end, respectively. It can be solved by BLT equations

$$\begin{aligned}\boldsymbol{\Psi}(x_0,\omega) &= \mathbf{M}(\mathbf{I}-\boldsymbol{\Gamma}\mathbf{M})^{-1}\boldsymbol{\Psi}^s\\ \boldsymbol{\Psi}^s &= \int_{x_0}^{x_1} e^{-\mathbf{D}(\omega)(x_1-x)}\big[\boldsymbol{\Psi}'(x,\omega) - \mathbf{N}(\omega)\boldsymbol{\Psi}(x,\omega)\big]dx.\end{aligned} \tag{16}$$

The vector parameters x_0 and x_1 are the boundary conditions. It is denoted as

$$\mathbf{x_0} = \begin{bmatrix}\mathbf{0}\\ \mathbf{d}\end{bmatrix} \in \mathbf{R}^{2N}, \quad \mathbf{x_1} = \begin{bmatrix}\mathbf{d}\\ \mathbf{0}\end{bmatrix} \in \mathbf{R}^{2N}. \tag{17}$$

The parameter $\mathbf{M}$ and $\boldsymbol{\Gamma}$ are represented as

$$\begin{aligned}\mathbf{M} &= \begin{bmatrix}\mathbf{0} & \boldsymbol{\rho}_1\\ \boldsymbol{\rho}_2 & \mathbf{0}\end{bmatrix} \in \mathbf{R}^{2N} \times \mathbf{R}^{2N}\\ \boldsymbol{\Gamma} &= \begin{bmatrix}e^{-\gamma_D} & \mathbf{0}\\ \mathbf{0} & e^{-\gamma_D}\end{bmatrix} \in \mathbf{R}^{2N} \times \mathbf{R}^{2N}\end{aligned} \tag{18}$$

where

$$\begin{aligned}\boldsymbol{\rho}_1 &= (\mathbf{Z_1} - \mathbf{Z_c})(\mathbf{Z_1} + \mathbf{Z_c})^{-1}\\ \boldsymbol{\rho}_2 &= (\mathbf{Z_2} - \mathbf{Z_c})(\mathbf{Z_2} + \mathbf{Z_c})^{-1}\\ \boldsymbol{\rho}_1, \boldsymbol{\rho}_2 &\in \mathbf{R}^N \times \mathbf{R}^N.\end{aligned} \tag{19}$$

In general case, the recursions could be written as

$$\begin{aligned}\boldsymbol{\Psi}^{(r+1)}(x,\omega) = e^{-\mathbf{D}(\omega)x}\mathbf{M}(\mathbf{I}-\boldsymbol{\Gamma}\mathbf{M})^{-1}\\ \int_{x_0}^{x_1} e^{-\mathbf{D}(\omega)(x_1-x)}\big[\boldsymbol{\Psi}'(x,\omega)\\ - \mathbf{N}(\omega)\boldsymbol{\Psi}^{(r)}(x,\omega)\big]dx\\ + \int_{x_0}^{x} e^{-\mathbf{D}(\omega)(x-x')}\big[\boldsymbol{\Psi}'(x',\omega)\\ - \mathbf{N}(\omega)\boldsymbol{\Psi}^{(r)}(x',\omega)\big]dx'.\end{aligned} \tag{20}$$

For the simplification of the cumbersome integral formula mentioned previously, bring in the convolution symbols which is defined as

$$e^{-\mathbf{D}(\omega)x} * \boldsymbol{\Psi}'(x,\omega) = \int_{x_0}^{x} e^{-\mathbf{D}(\omega)(x-x')}\boldsymbol{\Psi}'(x',\omega)dx'. \tag{21}$$

Then, (20) is converted into

$$\begin{aligned}\boldsymbol{\Psi}^{(r+1)}(x,\omega) &= e^{-\mathbf{D}(\omega)x}\mathbf{M}(\mathbf{I}-\boldsymbol{\Gamma}\mathbf{M})^{-1}\\ &\quad e^{-\mathbf{D}(\omega)x_1} * \big[\boldsymbol{\Psi}'(x_1,\omega) - \mathbf{N}(\omega)\boldsymbol{\Psi}^{(r)}(x_1,\omega)\big]\\ &\quad + e^{-\mathbf{D}(\omega)(x)} * \big[\boldsymbol{\Psi}'(x,\omega) - \mathbf{N}(\omega)\boldsymbol{\Psi}^{(r)}(x,\omega)\big].\end{aligned} \tag{22}$$

If we denote the parameter of (22) by

$$\begin{aligned}\mathbf{k_1}(\mathbf{x},\omega) &= e^{-\mathbf{D}(\omega)x}\\ \mathbf{k_2}(\mathbf{x},\omega) &= e^{-\mathbf{D}(\omega)x}\mathbf{M}(\mathbf{I}-\boldsymbol{\Gamma}\mathbf{M})^{-1}\\ \mathbf{k_3}(\mathbf{x},\omega) &= -e^{-\mathbf{D}(\omega)x}\mathbf{N}(\omega)\\ \mathbf{B}(\omega) &= \mathbf{M}(\mathbf{I}-\boldsymbol{\Gamma}\mathbf{M})^{-1}\end{aligned} \tag{23}$$

(22) can be written as

$$\begin{aligned}\boldsymbol{\Psi}^{(r+1)}(x,\omega) &= \big[\mathbf{k_2}(\mathbf{x},\omega)\mathbf{k_1}(\mathbf{x_1},\omega) * \boldsymbol{\Psi}'(x_1,\omega)\\ &\quad + \mathbf{k_1}(\mathbf{x},\omega) * \boldsymbol{\Psi}'(x,\omega)\big]\\ &\quad + \big[\mathbf{k_2}(\mathbf{x},\omega)\mathbf{k_3}(\mathbf{x_1},\omega) * \boldsymbol{\Psi}^{(r)}(x_1,\omega)\\ &\quad + \mathbf{k_3}(\mathbf{x},\omega) * \boldsymbol{\Psi}^{(r)}(x,\omega)\big].\end{aligned} \tag{24}$$

Taking notice of the two parts in the iterative formula (24), the one is a constant which only depends on the excitation of the field whereas the other is the iterative item. Denote that

$$\begin{aligned}\mathbf{S}^{(r+1)}(x,\omega) &= \boldsymbol{\Psi}^{(r+1)}(x,\omega) - \boldsymbol{\Psi}^{(r-1)}(x,\omega)\\ &= \mathbf{k_2}(\mathbf{x},\omega)\mathbf{k_3}(\mathbf{x_1},\omega) * \big[\boldsymbol{\Psi}^{(r)}(x_1,\omega)\\ &\quad - \boldsymbol{\Psi}^{(r-1)}(x_1,\omega)\big]\\ &\quad + \mathbf{k_3}(\mathbf{x},\omega) * \big[\boldsymbol{\Psi}^{(r)}(x,\omega) - \boldsymbol{\Psi}^{(r-1)}(x,\omega)\big]\\ &= \mathbf{k_2}(\mathbf{x},\omega)\mathbf{k_3}(\mathbf{x_1},\omega) * \mathbf{S}^{(r)}(x_1,\omega)\\ &\quad + \mathbf{k_3}(\mathbf{x},\omega) * \mathbf{S}^{(r)}(x,\omega)\\ \mathbf{S}^{(1)}(x,\omega) &= \boldsymbol{\Psi}^{(1)}(x,\omega).\end{aligned} \tag{25}$$

Then, we have the recursive equation defining all the $\mathbf{S}^{(r)}(x,\omega)$ iterates.

The first iteration in the DARIT-field method is to deal with the incoming EMP wave interacting with each line independently. So, the term $\mathbf{N}(\omega)$ in the first iteration is $\mathbf{0}$. The value of variable $\boldsymbol{\Psi}(x,\omega)$ after the first iteration is

$$\begin{aligned}\mathbf{S}^{(1)}(x,\omega) &= \boldsymbol{\Psi}^{(1)}(x,\omega)\\ &= \mathbf{k_2}(\mathbf{x},\omega)\mathbf{k_1}(\mathbf{x_1},\omega) * \boldsymbol{\Psi}'(x_1,\omega)\\ &\quad + \mathbf{k_1}(\mathbf{x},\omega) * \boldsymbol{\Psi}'(x,\omega)\\ &= \mathbf{k_2}(\mathbf{x},\omega)\int_{x_0}^{x_1} e^{-\mathbf{D}(\omega)(x_1-x)}\boldsymbol{\Psi}'(x,\omega)dx\\ &\quad + \int_{x_0}^{x} e^{-\mathbf{D}(\omega)(x-x')}\boldsymbol{\Psi}'(x',\omega)dx'.\end{aligned} \tag{26}$$

According to (25), at the second iteration and after, the recursions of $r+1$th iteration can be written as

$$\begin{aligned}\mathbf{S}^{(r+1)}(x,\omega) &= \mathbf{k_2}(\mathbf{x},\omega)\mathbf{k_3}(\mathbf{x_1},\omega) * \mathbf{S}^{(r)}(x_1,\omega)\\ &\quad + \mathbf{k_3}(\mathbf{x},\omega) * \mathbf{S}^{(r)}(x,\omega)\\ &= \mathbf{k_2}(\mathbf{x},\omega)\int_{x_0}^{x_1} e^{-\mathbf{D}(\omega)(x_1-x)}\\ &\quad \times \big[-\mathbf{N}(\omega)\big]\mathbf{S}^{(r)}(x,\omega)dx\\ &\quad + \int_{x_0}^{x} e^{-\mathbf{D}(\omega)(x-x')}\big[-\mathbf{N}(\omega)\big]\mathbf{S}^{(r)}(x',\omega)dx'.\end{aligned} \tag{27}$$

Taking the euclidean norms of the both sides in (27), it is converted into

$$\begin{aligned}\|\mathbf{S}^{(r+1)}(x,\omega)\| &= \|\mathbf{k_2}(\mathbf{x},\omega)\int_{x_0}^{x_1} e^{-\mathbf{D}(\omega)(x_1-x)}\big[-\mathbf{N}(\omega)\big]\\ &\quad \times \mathbf{S}^{(r)}(x,\omega)dx + \int_{x_0}^{x} e^{-\mathbf{D}(\omega)(x-x')}\big[-\mathbf{N}(\omega)\big]\\ &\quad \times \mathbf{S}^{(r)}(x',\omega)dx'\|\\ &\le \|\mathbf{k_2}(\mathbf{x},\omega)\|\int_{x_0}^{x_1}\|e^{-\mathbf{D}(\omega)(x_1-x)}\big[-\mathbf{N}(\omega)\big]\\ &\quad \times \mathbf{S}^{(r)}(x,\omega)dx\|\\ &\quad + \int_{x_0}^{x}\|e^{-\mathbf{D}(\omega)(x-x')}\big[-\mathbf{N}(\omega)\big]\mathbf{S}^{(r)}(x',\omega)dx'\|\\ &\le \|-\mathbf{N}(\omega)\|\Big[\|\mathbf{k_2}(\mathbf{x},\omega)\|\int_{x_0}^{x_1}\|e^{-\mathbf{D}(\omega)(x_1-x)}\|\\ &\quad \times \|\mathbf{S}^{(r)}(x,\omega)dx\| + \int_{x_0}^{x}\|e^{-\mathbf{D}(\omega)(x-x')}\|\|\\ &\quad \times \mathbf{S}^{(r)}(x',\omega)dx'\|\Big].\end{aligned} \tag{28}$$

Since the function $\|e^{-\mathbf{D}(\omega)(x_1-x)}\|$ and $\|e^{-\mathbf{D}(\omega)(x-x')}\|$ are continuous on the space, they have the upper bounds that we denote as $A_1(\omega)$ and $A(\omega)$, respectively. Noting that x_1 is a constant vector, and

$$x \in [x_0, x_1], \quad x' \in [x_0, x] \tag{29}$$

we have

$$\begin{aligned}\max\big(\big\|e^{-\mathbf{D}(\omega)(x_1-x)}\big\|\big) &= A_1(\omega) \le A(\omega)\\ &= \max\big(\big\|e^{-\mathbf{D}(\omega)(x-x')}\big\|\big).\end{aligned} \tag{30}$$

Then, (28) is converted into

$$\begin{aligned}\|\mathbf{S}^{(r+1)}(x,\omega)\| &\le \|-\mathbf{N}(\omega)\|A(\omega)\Big[\|\mathbf{k_2}(\mathbf{x},\omega)\|\\ &\quad \int_{x_0}^{x_1}\|\mathbf{S}^{(r)}(x,\omega)dx\| + \int_{x_0}^{x}\|\mathbf{S}^{(r)}(x',\omega)dx'\|\Big].\end{aligned} \tag{31}$$

In order to explore the upper bound of $\|\mathbf{S}^{(r+1)}(x,\omega)\|$ by the recursion (31), solving the $\|\mathbf{S}^{(1)}(x,\omega)\|$ first

$$\begin{aligned}\|\mathbf{S}^{(1)}(x,\omega)\| &= \|\mathbf{k_2}(\mathbf{x},\omega)\| \\ &\int_{x_0}^{x_1} \|e^{-\mathbf{D}(\omega)(x_1-x)}\boldsymbol{\Psi}'(x,\omega)\|dx \\ &+ \int_{x_0}^{x} \|e^{-\mathbf{D}(\omega)(x-x')}\boldsymbol{\Psi}'(x',\omega)\|dx' \\ &\le A(\omega)\Big[\|\mathbf{k_2}(\mathbf{x},\omega)\| \int_{x_0}^{x_1} \|\boldsymbol{\Psi}'(x,\omega)\|dx \\ &+ \int_{x_0}^{x} \|\boldsymbol{\Psi}'(x',\omega)\|dx'\Big]. \end{aligned} \tag{32}$$

Since the function $\|\boldsymbol{\Psi}'(x,\omega)\|$ is continuous on the space, it has an upper bound that we denote as $\Phi(\omega)$. Noting also that

$$\|\boldsymbol{\Psi}'(x,\omega)\| \le \Phi(\omega). \tag{33}$$

Then, (32) is converted into

$$\begin{aligned}\|\mathbf{S}^{(1)}(x,\omega)\| &\le A(\omega)\Phi(\omega)\left[\|\mathbf{k_2}(\mathbf{x},\omega)\| \int_{x_0}^{x_1} dx + \int_{x_0}^{x} dx'\right] \\ &\le A(\omega)\Phi(\omega)\big[\|\mathbf{k_2}(\mathbf{x},\omega)\|\|(x_1-x_0)\| \\ &\quad + \|(x-x_0)\|\big] \\ &\le A(\omega)\Phi(\omega)d\big[\|\mathbf{k_2}(\mathbf{x},\omega)\|+1\big]. \end{aligned} \tag{34}$$

According to (31) and (34), the upper bound of $\|\mathbf{S}^{(r)}(x,\omega)\|$ can be obtained

$$\begin{aligned}\|\mathbf{S}^{(r)}(x,\omega)\| &\le \Phi(\omega)\|\mathbf{N}(\omega)\|^{r-1}\big[A(\omega)\big]^r \\ &\big[\|\mathbf{k_2}(\mathbf{x},\omega)\|+1\big]^r \frac{d^r}{r!}. \end{aligned} \tag{35}$$

Note that the expression of upper bound of $\|\mathbf{S}^{(r)}(x,\omega)\|$ is the series form, the upper bound of $\|\boldsymbol{\Psi}(x,\omega)\|$ can be derived from the summation of it

$$\begin{aligned}\|\boldsymbol{\Psi}(x,\omega)\| &\le \|\lim_{n\to\infty}\sum_{r=1}^{n}\mathbf{S}^{(r)}(x,\omega)\| \\ &\le \lim_{n\to\infty}\sum_{r=1}^{n}\Phi(\omega)\|\mathbf{N}(\omega)\|^{r-1}\big[A(\omega)\big]^r \\ &\quad\times\big[\|\mathbf{k_2}(\mathbf{x},\omega)\|+1\big]^r\frac{d^r}{r!} \\ &= \frac{\Phi(\omega)}{\|\mathbf{N}(\omega)\|}\{e^{\{\|\mathbf{N}(\omega)\|A(\omega)d[\|\mathbf{k_2}(\mathbf{x},\omega)\|+1]\}}-1\}. \end{aligned} \tag{36}$$

B. Error Analysis

Based on the previous study, the expression of $\|\boldsymbol{\Psi}(x,\omega)\|$ is the series form. Then, the residual error after nth iteration is given by

$$\mathbf{R}^n(x,\omega) = \boldsymbol{\Psi}(x,\omega) - \sum_{k=1}^{n}\mathbf{S}^{(k)}(x,\omega) = \sum_{k=n+1}^{\infty}\mathbf{S}^{(k)}(x,\omega). \tag{37}$$

Taking the matrix norms of both sides in (37) and using the Lagrange Remainder Term, we get the following expression about upper bound of the residual error:

$$\begin{aligned}\|\mathbf{R}^n(x,\omega)\| &\le \sum_{k=n+1}^{\infty}\Phi(\omega)\|\mathbf{N}(\omega)\|^{k-1}\big[A(\omega)\big]^k \\ &\quad\times\big[\|\mathbf{k_2}(\mathbf{x},\omega)\|+1\big]^k\frac{d^k}{k!} \\ &= \Phi(\omega)\|\mathbf{N}(\omega)\|^n\big[A(\omega)\big]^{n+1}\big[\|\mathbf{k_2}(\mathbf{x},\omega)\|+1\big]^{n+1} \\ &\quad\times\frac{d^{n+1}}{(n+1)!}\Big\{e^{\left\{\|\mathbf{N}(\omega)\|A(\omega)d\left[\|\mathbf{k_2}(\mathbf{x},\omega)\|+1\right]\right\}}-1\Big\}. \end{aligned} \tag{38}$$

Above all, the relative error $\rho_n(\omega)$ of the DARIT-field method can be given by

$$\begin{aligned}\rho_n(\omega) &= \frac{\|\mathbf{R}^n(x,\omega)\|}{\|\boldsymbol{\Psi}(x,\omega)\|} \\ &= \|\mathbf{N}(\omega)\|^{n+1}\big[A(\omega)\big]^{n+1}\big[\|\mathbf{k_2}(\mathbf{x},\omega)\|+1\big]^{n+1}\frac{d^{n+1}}{(n+1)!} \\ &= \frac{\big\{A(\omega)\|\mathbf{N}(\omega)\|d\big[\|e^{-\mathbf{D}(\omega)x}\mathbf{B}(\omega)\|+1\big]\big\}^{n+1}}{(n+1)!} \\ &\le \frac{\big\{A(\omega)\|\mathbf{N}(\omega)\|d\big[A(\omega)\|\mathbf{B}(\omega)\|+1\big]\big\}^{n+1}}{(n+1)!}. \end{aligned} \tag{39}$$

Note that there are four parameters namely $\|\mathbf{N}(\omega)\|$, $A(\omega)$, $\|\mathbf{B}(\omega)\|$ and d in the expression of (39) which may influence the convergence speed.

The first parameter is $\|\mathbf{N}(\omega)\|$ which is derived from the nondiagonal part of propagation constant $\gamma(\omega)$. It describes the coupling intensity of the multiconductor lines. To research it, another parameter named coupling factor (CF) is used to describe the coupling degree of the MTLs is introduced. The larger the CF is, the more serious the coupling is. CF is defined by the per-unit-length (p.u.l.) inductance parameters as follows:

$$\mathrm{CF} = \max_{\substack{i,j\\ i\ne j}}\sqrt{\frac{l'^2_{ij}}{l'_{ii}l'_{jj}}} \tag{40}$$

where l'_{ij} is the (i,j)th cell of the $\mathbf{L}'$ matrix.

To study the relationship between $\|\mathbf{N}(\omega)\|$ and CF, model the microstrip structure with a symmetrical and lossy three conductors with the length, height, and diameter equal to 10 cm, 1 cm, and 1 mm which is above the lossy ground. The relative dielectric constant and electrical conductivity of ground are 10 and 0.01 S/m, respectively. The loads on both sides are 50 Ω. The frequency and amplitude of the excitation field are 1 GHz and 1 V/m, respectively. We set the distance between lines from 11 to 30 mm to make the CF range from 0.06 to 0.24. The relationship

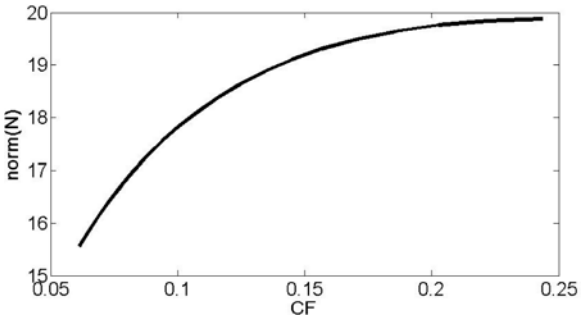

Fig. 2. Relationship between $\|\mathbf{N}(\omega)\|$ and CF.

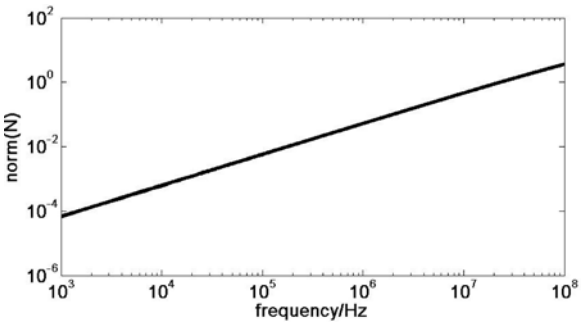

Fig. 3. Relationship between $\|\mathbf{N}(\omega)\|$ and frequency.

between $\|\mathbf{N}(\omega)\|$ and CF is shown in Fig. 2. It can be seen from the figure that $\|\mathbf{N}(\omega)\|$ increases with CF, in other words, the relative error increases monotonically with the CF.

Because of the frequency dependence of $\|\mathbf{N}(\omega)\|$, relationship between $\|\mathbf{N}(\omega)\|$ and frequency is also investigated. The microstrip structure modeling in this example is like the example mentioned previously except that the distance between lines is 2 cm which is constant and the frequency of excitation field ranges from 1 kHz to 100 MHz. The relationship between $\|\mathbf{N}(\omega)\|$ and frequency is shown in Fig. 3. Noting the curve in Fig. 3, the $\|\mathbf{N}(\omega)\|$ increases almost linearly with the frequency. In order to explore the essence of the convergence, transform the formula of (39) to

$$\rho_n(\omega) = \frac{\left\{A(\omega)\|\mathbf{N}(\omega)\lambda\|(d/\lambda)\left[A(\omega)\|\mathbf{B}(\omega)\| + 1\right]\right\}^{n+1}}{(n+1)!} \tag{41}$$

and study the relationship between $\|\mathbf{N}(\omega)\lambda\|$ and frequency as shown in Fig. 4. Note that the value of $\|\mathbf{N}(\omega)\lambda\|$in Fig. 4 is almost constant with the increase of frequency. It has only 5.3 dB decrease when the frequency ranges from 1 kHz to 100 MHz whereas the value of $1/\lambda$ increases 100 dB. From what mentioned previously, it can be said that the parameter $\|\mathbf{N}(\omega)\lambda\|$ has a monotonical relationship with CF and barely depends on other parameters such as frequency.

The second parameter is $\|\mathbf{B}(\omega)\|$ which is defined in (23) and mainly describes the influence factor of the terminal loads. To study the relationship between $\|\mathbf{B}(\omega)\|$ and loads, model the microstrip structure with a symmetrical and lossy three con-

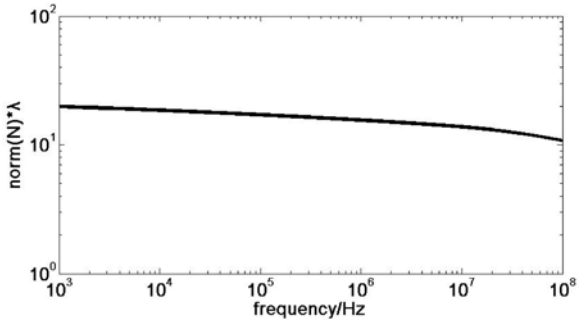

Fig. 4. Relationship between $\|\mathbf{N}(\omega)\lambda\|$ and frequency.

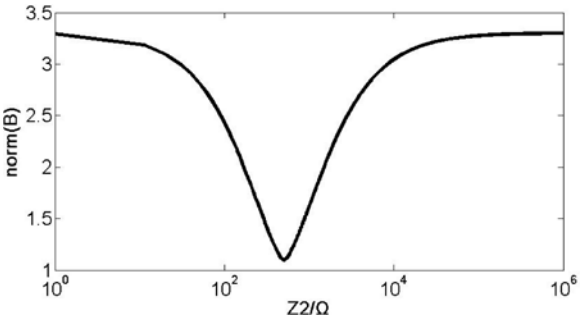

Fig. 5. Relationship between $\|\mathbf{B}(\omega)\|$ and Z_2.

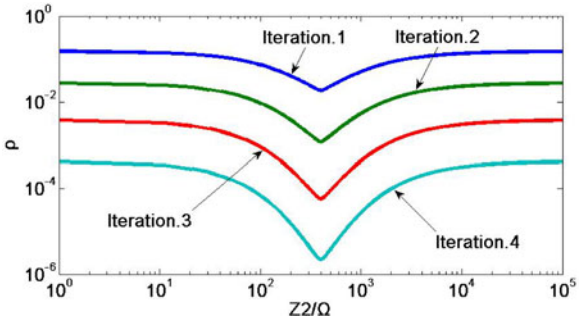

Fig. 6. Relationship between ρ and Z_2 after each iteration.

ductors with the length, height, diameter, and distance between lines equal to 10 cm, 1 cm, 1 mm, and 5 mm which is above the lossy ground. The relative dielectric constant and electrical conductivity of ground are 10 and 0.01 S/m, respectively. The frequency and amplitude of the excitation field are 100 MHz and 1V/m, respectively. The load Z_1 connected on near-end is matched load whereas the load Z_2 connected on far-end ranges from 1 Ω to 1 MΩ. The relationship between $\|\mathbf{B}(\omega)\|$ and Z_2 is shown in Fig. 5. From the figure, it can be seen that with the increase of Z_2, $\|\mathbf{B}(\omega)\|$ decreases first and then increases. To investigate in the relationship between load Z_2 and relative error ρ, plot the figure in Fig. 6. It can be seen from the plot that with the increase of Z_2, ρ decreases first and then increases, the curve shape of which is quite like the one in Fig. 5. Furthermore, when the value of Z_2 reaches approximately equal to the characteristic impedance of line, ρ reaches the minimum.

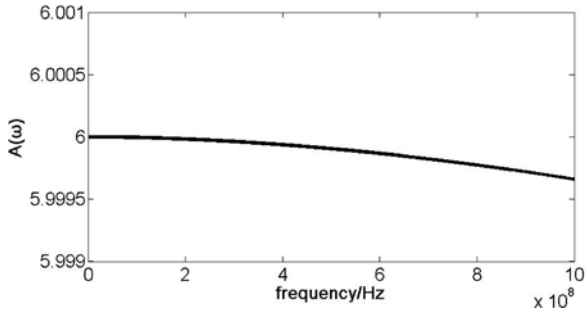

Fig. 7. Relationship between $A(\omega)$ and frequency.

It indicates that the terminal loads of line are key factors of the convergence.

The third parameter is $A(\omega)$. From the definition of $A(\omega)$, we know that it is a frequency-dependent parameter. To research the relationship between $A(\omega)$ and frequency, model the microstrip structure as in the example which describes the relationship between $\|\mathbf{N}(\omega)\|$ and frequency. The relationship between $A(\omega)$ and frequency is shown in Fig. 7. From the figure, we can see that $A(\omega)$ is almost constant with the increase of frequency.

The last parameter is the line length to wavelength ratio d/λ. It describes the relative geometric dimensioning between the MTLs and the excitation field. From the conclusions drawn above, the parameters $A(\omega)$, $\|\mathbf{B}(\omega)\|$, and $\|\mathbf{N}(\omega)\lambda\|$ in (41) are all independent on d or frequency, so the ratio parameter d/λ can be seen as an individual parameter which can have a direct influence on the relative error, in other words, it is an essence factor of the convergence.

From the expression of relative error mentioned previously and the parameters we have investigated, it can be concluded that, the key factors of convergence are CF, loads, and d/λ. The weaker the coupling is, the faster the convergence is. Furthermore, the larger the d/λ is, the slower the convergence is. Last, to reach convergence quickly, the loads on terminals should be approximately equal to the characteristic impedance of line. The conclusion will be validated with actual examples in the next section.

IV. Validation of the Convergence of DARIT-Field

In order to demonstrate the validity of the proposed DARIT-field algorithm for the calculation of EMP coupling to MTLs and the formula of convergence derived previously, we present some case studies which are commonly encountered. In all these examples, the MTLs were illuminated by the incoming EMP wave which was defined by IEC 61000-2-9

$$E(t) = E_0 k(e^{-\alpha t} - e^{-\beta t}) \tag{42}$$

where $E_0 = 5e4$, $k = 1.3$, $\alpha = 4e7$, $\beta = 6e8$.

First, we demonstrate the validity of DARIT-field to handle MTLs. A symmetrical and lossy nine conductors microstrip structure with length of 1 cm, height of 1 mm, diameter of 0.1 mm, and distance between lines of 1.5 mm which is above the lossy ground is considered. The relative dielectric constant and electrical conductivity of ground are 10 and 0.01 S/m, respectively. The loads on sides are 50 Ω at near-end and 1 pF at far-end. Fig. 8 shows a sample of the waveforms computed with DARIT-field (after Iteration 4) compared to the waveforms computed from the conventional stamp method [1], [10]. As seen from the plots, the results are in very good agreement.

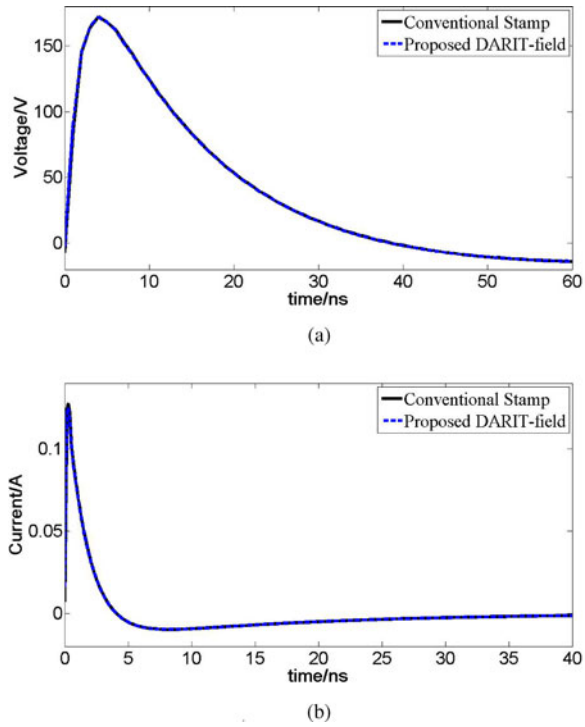

Fig. 8. Induced waveform of far-end of line #1. (a) Voltage waveform. (b) Current waveform.

Then, we present three examples to validate the formula of convergence derived before. The first example demonstrates the iterative error with different CFs. The second example illustrates the relationship between iterative error and the terminal loads of line. The third example illustrates the relationship between iterative error and the line length to wavelength ratio d/λ.

A. Example 1: The Relationship Between Iteration Error and the CF

The purpose of this example is to quantitatively illustrate the relative error of the DARIT-field as a function of different CFs. Since the relative error $\rho_n(\omega)$ mentioned previously is deduced by the euclidean norms, it represents the global error of the method. In order to propose another equivalent parameter which can be easily calculated, a relative error ϵ based on energy norm in frequency domain is defined as follows:

$$\begin{aligned}\epsilon &= \left| \frac{\int_{f_{\min}}^{f_{\max}} |S_1(\zeta)|^2 d\zeta - \int_{f_{\min}}^{f_{\max}} |S_2(\zeta)|^2 d\zeta}{\int_{f_{\min}}^{f_{\max}} |S_1(\zeta)|^2 d\zeta} \right| \\ &\cong \left| \frac{\sum_{k=1}^{N_f} |S_1(f_k)|^2 - \sum_{k=1}^{N_f} |S_2(f_k)|^2}{\sum_{k=1}^{N_f} |S_1(f_k)|^2} \right| \end{aligned} \tag{43}$$

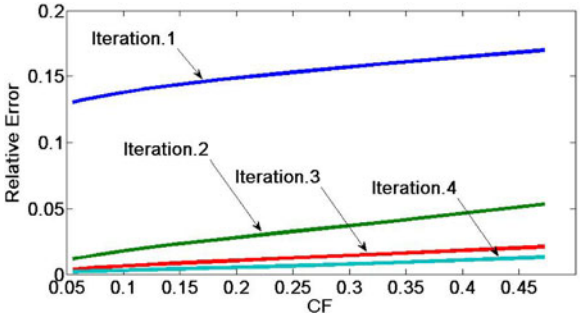

Fig. 9. Dependence of relative error on CF.

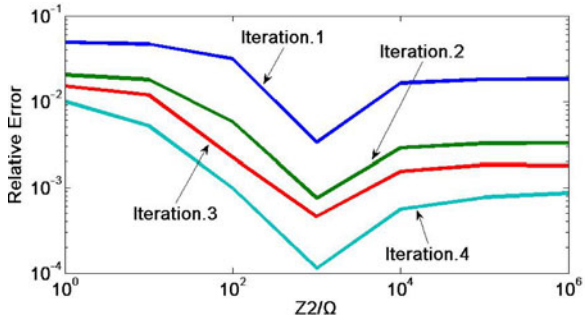

Fig. 10. Dependence of relative error on loads after each iteration.

where N_f is the number of sampling points in the frequency domain and f_k is the value of frequency at the kth sampling point. S_1 and S_2 represent the reference value obtained by the conventional stamp method and the value obtained by the proposed method, respectively.

To model the microstrip structure, a symmetrical and lossy three conductors above the lossy ground are considered. The length, height, and diameter of lines are equal to 10 cm, 1 cm, and 1 mm, respectively. The relative dielectric constant and electrical conductivity of ground are 10 and 0.01 S/m, respectively. The loads on both sides are 50 Ω. We produce ten cases with CFs from 0.05 to 0.45 by changing the distance between lines from 5 to 35 mm. The waveform of exciting source is the IEC HEMP pulse with $\alpha = 0°$, $\psi = 30°$, and $\phi = 0°$. Fig. 9 shows the relative error with the varied CFs after iteration 1, 2, 3, 4, respectively. As seen from the plot, the relative error increases with the increase of the CF, the curve shape of which is quite like the conclusions mentioned previously.

B. Example 2: The Relationship Between Convergence and Loads

Since the reflection coefficients in the solutions are different from the line parameters as they depend on both the line properties and the nature of the termination impedance, the objective of this example is to illustrate the relationship between convergence and terminal loads. A symmetrical and lossy three conductors microstrip structure with length of 10 cm, height of 1 cm, diameter of 1 mm, and distance between lines of 5 mm which is above the lossy ground is considered. The loads on near-end are equal to characteristics impedance and on far-end varied of 1, 10, 100, 1000, 10 000, 100 000, and 1000 000 Ω. The relative dielectric constant and electrical conductivity of ground are 10 and 0.01 S/m, respectively. The waveform of exciting source is the IEC HEMP pulse with $\alpha = 0°$, $\psi = 30°$, and $\phi = 0°$. Fig. 10 shows the dependence of relative error on loads after iterations 1–4. As seen clearly from the plot, the relative error decreases first and then increases with the increase of loads. Meanwhile, it becomes smaller after each iteration, which corresponds to Fig. 6.

Note that the notation of y-axis ρ in Fig. 6 represents the error which is derived from the formula derivation, whereas the notation of y-axis relative error in Fig. 10 is derived from the calculation result from the actual computational example. Strictly speaking, ρ is different from relative error, although the ρ in Fig. 6 and the relative error in Fig. 10 are related. The difference between them mainly results from the inequality zoom tasks in the formula derivation process of ρ. But since the inequality zoom level in formula derivation is controlled below a reasonable extent, ρ still represents the nature of relative error qualitatively, and the validation mentioned previously provides the proof for this conclusion.

C. Example 3: The Relationship Between Convergence and the Line Length to Wavelength Ratio

This example illustrates the line length to wavelength ratio d/λ which is an innate character of the convergence. For illustrating quantitatively, we set two groups of parameters and calculate the relative error in frequency domain between the proposed algorithm and the conventional method. The relative error in frequency domain $\epsilon_f(\omega)$ is defined as

$$\epsilon_f(\omega) = \frac{|S_{\text{iter}}(\omega) - S_{\text{conv}}(\omega)|}{|S_{\text{conv}}(\omega)|} \tag{44}$$

where S_{iter} represents the result from the iteration method, S_{conv} represents the result from the conventional method.

Then, we calculate the $\epsilon_f(\omega)$ with the two groups of parameters and make a comparison between them. The comparison makes sense if the $d/\lambda_{\min}$ in these two groups keeps the same. The model in the first group includes three symmetrical and lossy conductors which are excited by the continuous electromagnetic wave of amplitude of 1 V/m and the frequency range of the source is from 100 kHz to 100 MHz with length of 10 cm, height of 1 cm, diameter of 1 mm, and distance between lines is 1 cm above the lossy ground. The second group is the same as the first except that the lower bound frequency, upper bound frequency, and length change to 50 kHz, 50 MHz, and 20 cm, respectively. Fig. 11(a) shows the relationship between relative error in frequency domain and d/λ after each iteration when $d = 10$ cm. It can be seen from the figure that with the increases of d/λ, the relative error also increases. Fig. 11(b) shows the relationship of relative error in frequency domain and d/λ after each iteration when $d = 20$ cm. It can be seen from the plot that the value of relative error is almost the same as in Fig. 11(a) at the same point of d/λ though their lengths are different. It

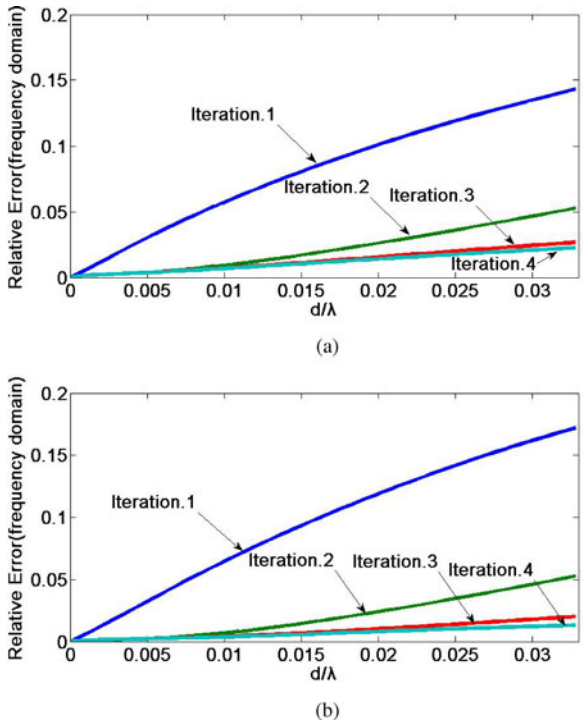

Fig. 11. Relationship between relative error in frequency domain and d/λ after each iteration with different d. (a) $d = 10$ cm. (b) $d = 20$ cm.

indicates that the convergence is only dependent on the ratio parameter d/λ rather than only on d or frequency.

V. Summary and Conclusion

This paper discusses the convergence of the DARIT-field which is an iterative approach (Jacobi iteration) to predict EMP coupling to MTLs. An expression of relative error after nth iteration has been derived by combining the two equations of telegrapher's equations to a matrix equation and exploring the upper bound of the relative error by using the matrix norm. From the theoretical analysis and the validation examples, we can get some conclusions. First, the relative error increases with CF. Second, the relationship between the convergence and terminal loads is nonlinear. With the increase of terminal loads, the relative error presents a down and up trend whereas the lowest value turns out when the terminal loads equal to characteristic impedance of line. Finally, the iteration relative error is a monotone increasing function of the line length to wavelength ratio d/λ. Above all, the convergence speed is depending on the CF, terminal loads, and the line length to excitation field wavelength ratio (d/λ). These convergence properties allow the users to make a compromise between computational cost and accuracy by selecting the number of iterations.

References

[1] C. R. Paul, *Analysis of Multiconductor Transmission Lines*, 2nd Ed., New York, NY, USA: Wiley, 2008.

[2] F. M. Tesche, M. V. Ianoz, and T. Karlsson, *EMC Analysis Methods and Computational Models*. New York, NY, USA: Wiley, 1997.

[3] C. R. Paul, "Solution of the transmission-line equations under the weak-coupling assumption," *IEEE Trans. Electromagn. Compat.*, vol. 44, no. 3, pp. 413–423, Aug. 2002.

[4] C. E. Baum, "Low- and high-frequency solutions of the telegrapher equations for nonuniform multiconductor transmission lines," in *Proc. IEEE Int. Symp. Electromagn. Compat.*, Jul. 2007, pp. 1–14.

[5] F. Canavero and I. Maio, "Transient simulation of lossy multiconductor interconnects," in *Proc. Int. Symp. Electromagn. Compat.*, May 21–23, 1997, pp. 243–246.

[6] C. R. Paul, "Computation of crosstalk in a multiconductor transmission line," *IEEE Trans. Electromagn. Compat.*, vol. EMC-23, no. 4, pp. 352–358, Nov. 1981.

[7] C. R. Paul, "Literal solutions for time-domain crosstalk on lossless transmission lines," *IEEE Trans. Electromagn. Compat.*, vol. 34, no. 4, pp. 433–444, Nov. 1992.

[8] I. Maio and F. Canavero, "Transient field coupling and crosstalk in lossy lines with arbitrary loads," *IEEE Trans. Electromagn. Compat.*, vol. 37, no. 4, pp. 599–606, Nov. 1995.

[9] S. Grivet-Talocia, H.-M. Huang, A. E. Ruehli, F. Canavero, and I. M. Elfadel, "Transient analysis of lossy transmission lines: an efficient approach based on the method of Characteristics," *IEEE Trans. Adv. Packag.*, vol. 27, no. 1, pp. 45–56, Feb. 2004.

[10] R. Achar and M. S. Nakhla, "Simulation of high-speed interconnects," *Proc. IEEE*, vol. 89, no. 5, pp. 693–728, May 2001.

[11] Y.-Z. Xie, F. Canavero, T. Maextri, and Z.-J. Wang, "Crosstalk analysis of multiconductor transmission lines based on distributed analytical representation and iterative technique," *IEEE Trans. Electromagn. Compat.*, vol. 52, no. 3, pp. 712–727, Aug. 2010.

[12] Y.-Z. Xie, J. Guo, and F. Canavero, "Analytic iterative solution of electromagnetic pulse coupling to multiconductor transmission lines," *IEEE Trans. Electromagn. Compat.*, vol. 55, no. 3, pp. 451–466, Jun. 2013.

[13] C. E. Baum, T. K. Liu, and F. M. Tesche, "On the analysis of general multiconductor transmission line networks," Airforce Weapons Laboratory, Albuquerque, NM, USA, Interaction Note 350, 1978.

[14] N. Nakhla, A. Ruehli, M. Nakhla, and R. Achar, "Simulation of coupled interconnects using waveform relaxation and transverse partitioning," in *Proc. IEEE 13th Topical Meeting Electr. Performance Electron. Packag.*, Oct. 2004, pp. 25–28.

[15] I. M. Elfadel, "Convergence of transverse waveform relaxation for the electrical analysis of very wide transmission line buses," *IEEE Trans. Comput.-Aided Design Integr. Circuits Syst.*, vol. 28, no. 8, pp. 1150–1161, Aug. 2009.

[16] N. Nakhla, A. E. Ruehli, M. S. Nakhla, R. Achar, and C.-Z. Chen, "Waveform relaxation techniques for simulation of coupled interconnects with frequency-dependent parameters," *IEEE Trans. Adv. Packag.*, vol. 30, no. 2, pp. 257–269, Feb. 2007.

[17] F. Wenger, T. Gustafsson, and L. J. Svensson, "Perturbation theory for inhomogeneous transmission lines," *IEEE Trans. Circuits Syst.-1*, vol. 49, no. 3, pp. 289–297, Mar. 2002.

[18] Y. Bayram and J. L. Volakis, "A Generalized MoM-SPICE iterative technique for field coupling to multiconductor transmission lines in presence of complex structures," *IEEE Trans. Electromagn. Compat.*, vol. 47, no. 2, pp. 234–246, 2005.

[19] R. Achar, M. S. Nakhla, H. S. Dhindsa, A. R. Sridhar, D. Paul, and N. M. Nakhla, "Parallel and scalable transient simulator for power grids via waveform relaxation (PTS-PWR)," *IEEE Trans. Very Large Scale Integr. Syst.*, vol. 19, no. 2, pp. 319–332, Feb. 2011.

[20] Y.-Z. Xie, F. Canavero, etc, "Analytic iterative approach to crosstalk analysis of multiconductor transmission lines," in *Proc. Eur. Electromagn. Compat.*, 2010, pp. 775–780.

[21] M. A. Farhan, N. M. Nakhla, M. S. Nakhla, R. Achar, and A. E. Ruehli, "Overlapping partitioning techniques for simulation of strongly coupled distributed interconnects," *IEEE Trans. Components, Packag. Manuf. Technol.*, vol. 2, no. 7, pp. 1193–1201, Jul. 2012.

[22] E. Lelarasmee, A. E. Ruehli, and A. L. Sangiovanni-Vincentelli, "The waveform relaxation method for time-domain analysis of large-scale integrated circuits," *IEEE Trans. Comput.-Aided Design Integr. Circuits Syst.*, vol. 1, no. 3, pp. 131–145, Jul. 1982.

[23] H. Dhindsa, A. Sridhar, R. Achar, M. Nakhla, and D. Paul, "Transient analysis of power grid networks via waveform relaxation techniques," in *Proc. Int. Microw. Workshop Ser. Signal Integrity High-Speed Interconnects*, Feb. 2009, pp. 91–94.

[24] A. R. Sridhar, N. M. Nakhla, R. Achar, M. S. Nakhla, and A. E. Ruehli, "Fast EMI analysis via transverse partitioning and waveform relaxation," *IEEE Trans. Electromagn. Compat.*, vol. 51, no. 2, pp. 358–371, May 2009.

[25] F. Y. Chang, "The generalized method of characteristics for waveform relaxation analysis of lossy coupled transmission lines," *IEEE Trans. Microw. Theory Tech.*, vol. 37, no. 12, pp. 2028–2038, Dec. 1989.

[26] F. Y. Chang, "Transient simulation of nonuniform coupled lossy transmission lines characterized with frequency-dependent parameters: Part I. Waveform relaxation analysis," *IEEE Trans. Circuits Syst. I: Fundamental Theory Appl.*, vol. 39, no. 8, pp. 585–603, Aug. 1992.

[27] S. Roy and A. Dounavis, "Longitudinal-partitioning-based waveform relaxation for efficient analysis of distributed transmission-lines," *IEEE Trans. Microw. Theory Techn.*, vol. 60, no. 3, pp. 451–463, Mar. 2012.

[28] S. Roy and A. Dounavis, "Delay-Extraction-Based waveform relaxation algorithm for fast transient analysis of power distribution networks," *IEEE Trans. Components, Packag. Manuf. Technol.*, vol. 2, no. 12, pp. 2044–2056, Dec. 2012.

[29] S. Roy and S. A. Dounavis, "Parallel transient simulation of package/board power distribution networks based on a 2-D overlapping partitioning methodology," *IEEE Trans. Components, Packag. Manuf. Technol.*, vol. 3, no. 12, pp. 2101–2112, Dec. 2013.

[30] S. Roy, A. Beygi, and A. Dounavis, "Electromagnetic interference analysis of multiconductor transmission line networks using longitudinal partitioning-based waveform relaxation algorithm," *IEEE Trans. Electromagn. Compat.*, vol. 55, no. 2, pp. 395–406. Apr. 2013.

[31] N. Nakhla, M. S. Nakhla, and R. Achar, "Simplied delay extraction based passive transmission line macromodeling algorithm," *IEEE Trans. Adv. Packag.*, vol. 33, no. 2, pp. 498–509, May 2010.

[32] H. Yan, L. P. Yan1, X. Zhao1, H. J. Zhou, and K. M. Huang, "Analysis of electromagnetic field coupling to microstrip line connected with nonlinear components," *Progress Electromagn. Res. B*, vol. 51, pp. 291–306, 2013.

[33] S. Roy and A. Dounavis, "Waveform relaxation based analysis of noise propagation in power distribution networks propagation in power distribution networks," in *Proc. IEEE 20th Conf. Electr. Performance Electron. Packag. Syst.*, 2011, pp. 255–258.

[34] M. A. Khaleel, A. E. Ruchli, and M. J. Gander, "Optimized waveform relaxation methods for longitudinal partitioning of transmission lines," *IEEE Trans. Circuits Syst. I*, vol. 56, no. 8, pp. 1732–1743, Aug. 2009.

[35] G. Shinh, R. Achar, N. Nakhla, M. Nakhla, and I. Erdin, "Simplified macromodel of MTLs with incident fields (SiMMIF)," *IEEE Trans. Electromagn. Compat.*, vol. 50, no. 2, pp. 375–389, May 2008.